RESEARCH ARTICLE

Key Points:
- Observation of one FTE generated by an intensification of a pre-existing reconnection line
- A strong antiparallel current inside the FTE indicates its approximately force-free nature
- The FTE presents a core structure with electron scale

Correspondence to:
M. Silveira,
marcos.silveira@nasa.gov

Flux Transfer Event With an Electron-Scale Substructure Observed by the Magnetospheric Multiscale Mission

M. V. D. Silveira[1,2] [ID] , **D. G. Sibeck[1]** [ID] , **S. H. Lee[1,2]** [ID] , **D. Koga[3,4]** [ID] , **V. M. Souza[3]** [ID] , **W. D. Gonzalez[3]** [ID] , and **C. T. Russell[5]** [ID]

[1]NASA Goddard Space Flight Center, Greenbelt, MD, USA, [2]Department of Physics, Catholic University of America, Washington, DC, USA, [3]National Institute for Space Research, São José dos Campos, Brazil, [4]State Key Laboratory of Space Weather, National Space Science Center, Chinese Academy of Sciences, Beijing, China, [5]Department of Earth and Space Sciences, University of California, Los Angeles, CA, USA

Abstract On 12 November 2015 the Magnetospheric Multiscale (MMS) spacecraft traversed the magnetopause from the magnetosphere to the magnetosheath encountering evidence of magnetic reconnection and a tiny flux transfer event (FTE) on the magnetosheath side of the magnetopause boundary layer. The FTE exhibited a large negative-positive bipolar variation in the normal magnetic field component (B_N), an enhanced (negative) north-south component direction (B_L), and a variation in the third component B_M resembling a "W" shape with negative values close to the edges and positive values near the center. Using the tetrahedron formation, we estimate that the FTE moved southward and duskward with a speed of $V_{FTE} = 324$ km/s. The FTE size in the transverse direction is 518 km, which corresponds to 4.42 ion gyroradii. We identify an internal layer where the electron bulk flow velocity exhibits different behaviors at each of the four spacecraft and the current density was more intense at two spacecraft. Within the FTE's core region, the ion bulk flow behavior was similar for all four spacecraft. Using the velocity obtained from timing analysis, we estimate a dimension of this core region to be 181.4 km, which corresponds to 1.5 ion gyroradii. It is evident that the internal region is not large enough to affect the ion behavior but can do so for electrons. We conclude that the FTE's core is an electron-scale substructure.

1. Introduction

Magnetic reconnection is a fundamental phenomenon in plasma physics. It is defined as a topological restructuring of magnetic fields due to changes in magnetic connectivity (Priest & Forbes, 2000). In the Earth's magnetosphere, magnetic reconnection is responsible for mass, energy, and momentum exchange between the magnetosphere and solar wind (Dungey, 1961). Depending on the solar wind conditions, magnetic reconnection can be steady or transient in time and large scale or patchy in space (Heppner, 1972; Paschmann et al., 2013; Phan et al., 2004; Retinò et al., 2005; Russell & Elphic, 1978). Its consequences can be observed as a disturbance of plasma convection in the magnetosphere, injection of particles into the high-latitude ionosphere, and magnetic field variations measured on the ground (Birn et al., 2012; Lockwood & Smith, 1994; Sanny et al., 2002).

Flux transfer events (FTEs) have been interpreted as a result of transient magnetic reconnection, and they are frequently observed in the vicinity of the Earth's magnetopause (Russell & Elphic, 1978, 1979), as well as at other planets (Jasinski et al., 2016; Russell, 1995). FTEs are structures connecting the magnetosheath to the magnetosphere, allowing the transfer of plasma across the magnetopause. They are generated in the reconnection site and dragged off by pressure gradients and Lorentz forces along with the outflowing plasma. During their motion, FTEs create disturbances in the surrounding plasma and magnetic field orientation. FTE signatures are most readily identified when placed in the boundary normal coordinate system introduced by Russell and Elphic (1978). (It will be discussed in section 3.) In this coordinate system, events can be commonly recognized by a bipolar variation in the magnetic field component B_N normal to the nominal magnetopause boundary centered on a magnetic field strength enhancement. The polarity sign of the variation in the B_N component depends on the relative motion between the FTE and the observing spacecraft. A positive-negative B_N variation is referred to as *direct* or *standard* and is due to an FTE moving northward from the reconnection line. On the other hand, a negative-positive B_N polarity is consistent with an FTE

moving southward from the reconnection line, and in this case it is named *reverse* (Rijnbeek et al., 1982). In addition to the magnetic field, FTEs can exhibit plasma features such as mixtures of magnetosheath and magnetospheric plasma, accelerated ion and electron bulk flows, and temperatures and number densities with intermediate values between the two regions (Paschmann et al., 1982; Russell & Elphic, 1978).

Surveys have reported that FTEs can be observed along the entire dayside magnetopause surface although there is no general consensus where they are generated nor how far they can travel before evolving or disappearing. They occur preferentially during intervals when the north-south component B_Z of the interplanetary magnetic field (IMF) is southward, corroborating the hypothesis that FTEs are generated by magnetic reconnection (Berchem & Russell, 1984; Rijnbeek et al., 1984). The spatial dimensions of the structure can reveal the flux content and energy transferred to the magnetosphere and also the size of the disturbance they can generate locally (Sibeck & Lin, 2010). Fear et al. (2008) used multipoint measurements to estimate that FTEs observed by the Cluster mission (Escoubet et al., 2001) extended for at least 10,000 km in the azimuthal (approximately east-west) direction, which corresponded to the maximum separation among the spacecraft for that period. Several other studies addressed FTEs cross sections. They reported scale sizes ranging from 1 to several Earth radii (R_E) (Rijnbeek et al., 1984; Russell & Elphic, 1978; Saunders et al., 1984). However, numerical simulations have suggested the frequent occurrence of small flux ropes and their importance for particle acceleration during reconnection (Chen et al., 2008; Drake et al., 2006). Observations of such small structures by previous missions were limited by the instrument time resolution (Fermo et al., 2011). The limited resolution enables FTEs to be studied that had durations no shorter than 1 min (Elphic, 2013; Smith et al., 1986). Later, cases of small FTEs were reported by Fear et al. (2007) and Owen et al. (2001) with dimensions on the order of 0.8 R_E presenting internal core region structures with spatial scales of the order of ~600 km. Recently, work by Akhavan-Tafti et al. (2018) reported Magnetospheric Multiscale (MMS) observations of FTEs with nominal diameters of 1,700 km (~30 ion inertial lengths) and a mean magnetic flux content of 100 kWb.

How FTEs are generated by reconnection is not totally clear, and some of the models that address this question differ in the number of reconnection lines involved and the length of these reconnection lines. Russell and Elphic (1978) introduced the elbow-shape model where an FTE is generated by one short reconnection X-line enabling the connection of magnetosheath and magnetospheric magnetic field lines. Lee and Fu (1985) invoke multiple reconnection lines to generate FTEs with near circular cross sections. The extent in the azimuthal dimension is determined by the reconnection X-line length. A third model based on one reconnection line was proposed by Southwood et al. (1988) and Scholer (1988). Different from the elbow-shape model, in this model the azimuthal dimension lies along the reconnection line and the FTE has the shape of a bulge. A complete review of these models can be found in Fear et al. (2008). Only with analysis of the entire magnetopause crossing and the magnetic reconnection itself it is possible to evaluate which model best explains individual FTEs.

The MMS mission (Burch et al., 2016) was launched in 2015 with the goal of revealing the mechanisms of magnetic reconnection on kinetic scales. The small distances between the spacecraft and the high time resolution of the instruments enable observations of structures like small FTEs and substructures within them. Eastwood et al. (2016) used MMS observations to report FTEs with cross section of 0.17 R_E (approximately 7 ion inertial length) where ions exhibit a non-frozen-in behavior. Hwang et al. (2016) also reported a transverse small-scale structure with counterstreaming electrons suggesting the existence of open field lines at the FTE's core. Ion-scale FTEs with multiscale coupling have also been observed at the magnetopause and in the turbulent magnetosheath (Huang et al., 2016; Zhong et al., 2018). Akhavan-Tafti et al. (2018) investigated ion-scale FTEs at the subsolar magnetopause, which exhibit a force-free nature, whereas Zhao et al. (2016) and Farrugia et al. (2018) reported observations of non-force-free FTE structures. Other studies connecting small transient structures, FTE-like and flux ropes, with energy dissipation using MMS data, have been reported on the dayside (Jiang et al., 2019) and in the magnetotail (Huang et al., 2019).

We present MMS spacecraft observations of a magnetopause crossing with evidence of magnetic reconnection and a magnetosheath excursion with enhancements in the total magnetic field strength centered on bipolar B_N signatures on four occasions on 12 November 2015. The first of such magnetic field enhancements was observed at 07:06:00 UT and the other three between 07:08:00 and 07:09:00 UT. These magnetic field variations along with local plasma acceleration are consistent with the signatures of FTEs. The largest

variation in the magnetic field B_N component was observed during the first FTE, which will be discussed in detail in this paper.

2. Data

We use data from the MMS (Burch et al., 2016) for magnetopause observations and the Advanced Composition Explorer (ACE) as a solar wind monitor (Stone et al., 1998). During Phase 1A, when the observations were made, the MMS mission comprises four spacecraft in highly elliptical equatorial orbits. During this particular event MMS spacecraft were arranged in a tetrahedral formation with separations between 12 and 20 km and with a tetrahedron quality factor of TQF = 0.8 (TQF equal to unity represent a perfect tetrahedron. For more details, see Fuselier et al., 2016). The spacecraft are identically equipped with fluxgate magnetometers (FGM) (Russell et al., 2016), fast plasma investigations (FPI) (Pollock et al., 2016), energetic particle detectors (EPDs) (Mauk et al., 2016), and electric field instruments in the form of the spin-plane double probe (SDP) (Lindqvist et al., 2016) and the axial double probe (ADP) (Ergun et al., 2016). We used the magnetic field data from the FGM at survey and burst resolutions with cadences of 62.5 and 7.81 ms, respectively. For the plasma data, we used the FPI instrument with a cadence of 4.5 s in survey data for the period that contains the magnetopause crossing and for the FTE analysis we used the highest resolution available, that is, 150 ms for ions (dual ion spectrometer) and 30 ms for electrons (dual electron spectrometer) (burst data). The electric field data used have a time resolution of 122 μs.

Using the solar wind speed observed by ACE satellite, we estimate the time in which the magnetic structures spend to travel from the L1 libration point to the nose of the bowshock (not shown here). Assuming the magnetic field traveling on a planar surface with the solar wind speed, we found an average time shift of 53.6 min. After time shifting ACE's magnetic field data to the bowshock nose location, we performed a 5 min average of each IMF component to determine the prevalent IMF orientation immediately before the observed FTE. The averaging interval thus went from 07:01 to 07:06 UT, and the calculated IMF vector is (–2.24, –1.07, –2.07) nT in geocentric solar magnetospheric (GSM) coordinate system. The magnetic shear angle of 155° between the time-shifted IMF and the magnetospheric magnetic field favors component reconnection in the magnetopause's subsolar region (Gonzalez & Mozer, 1974). However, when we consider the magnetic field in the magnetosheath region adjacent to the magnetopause (between 07:05:27 and 07:05:39 UT), as observed by MMS, the local shear angle is 166°. Earth's magnetic dipole tilt is –25.3° for this event, according to the Tsyganenko (1996) model.

3. Observations

3.1. Magnetopause Crossing

On 12 November 2015 the MMS mission traversed the magnetopause from the magnetosphere to the magnetosheath on an outbound trajectory. During the crossing, MMS observed a magnetic field rotation combined with accelerated flows, which are consistent with evidence for magnetic reconnection and also FTEs on the magnetosheath side of the magnetopause boundary. To describe the complete scenario, Figures 1a–1g present an overview of magnetic field and plasma parameters observed by the MMS3 during the 10 min following 07:02:00 UT. On the right side of Figure 1, that is, on panels h and i, sketches are shown with a proposed time sequence of the events observed by MMS. We omitted observations for the other MMS spacecraft because they show similar features at the survey data resolution, as expected for such small spacecraft separations.

We employed minimum variance analysis on the magnetic field vectors (MVAB) (Sonnerup & Scheible, 1998) to determine the normal component in the boundary coordinate system during the magnetopause crossing. The MVAB technique was employed on each spacecraft individually during their magnetopause crossings for different time intervals. The spacecraft were located near to the subsolar region at (11.5, 2.2, –1.7) R_E in the GSM coordinate system. At this location we expect the boundary coordinate system to lie near to GSM coordinates with the **N** component pointing in the direction normal to the magnetopause current sheet. We choose the MVAB result from MMS3 based on the best eigenvalues ratio ($\lambda_{max}/\lambda_{int} = 25.2$ and $\lambda_{int}/\lambda_{min} = 6.35$) in the time interval 07:04:21–07:04:40 UT, as marked by the dashed red lines (3 and 4) in Figure 1. The selected interval contains 304 measurements. To compute the boundary coordinate system (LMN), we choose the eigenvector with the maximum variance as the (northward) component (**L**). The third component is given by the intermediate variance eigenvector, (**M**), pointing dawnward.
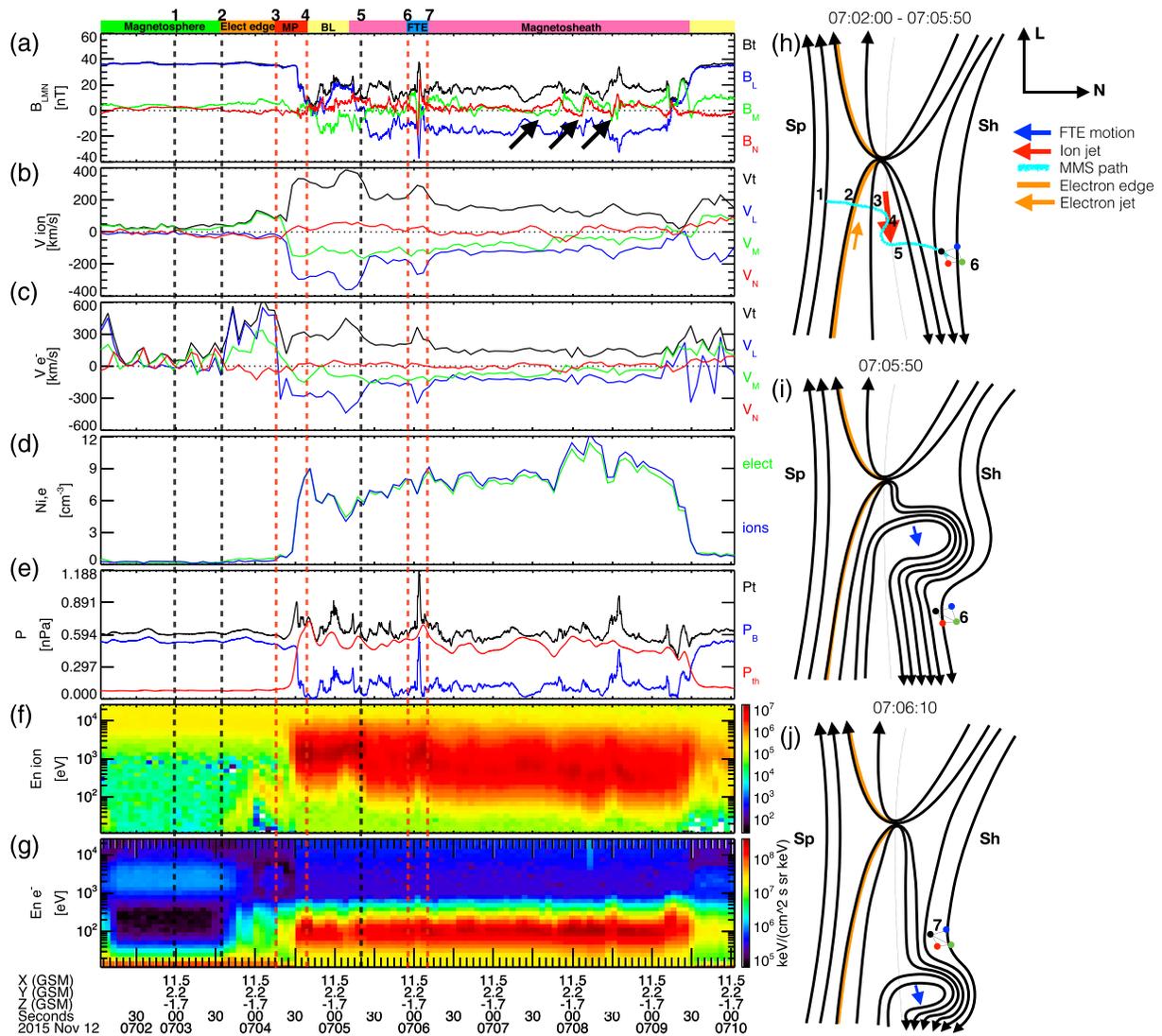
Figure 1. From (a)–(g) is shown an overview of magnetic and plasma parameters observed by MMS3 during 10 min period following 07:02:00 UT. (h)–(j) depict sketches of MMS trajectories and the encounter with the FTE as interpreted from the in situ observations. The numbered vertical dashed lines correspond to the regions observed by MMS, and they represented on panels (h) to (j). Further explanation can be found in the text.

We also determined the boundary coordinate system using the nominal magnetopause location obtained from the Shue et al. (1998) model. In a similar way it is possible to calculate the normal vector to the magnetopause at any given location thus providing the **n** component. The dawn-dusk component **m** is calculated by $\mathbf{m} = \mathbf{n} \times \mathbf{z}_{gsm}$, where $\mathbf{z}_{gsm} = [0, 0, 1]$ in GSM and the north-south **l** component is calculated by $\mathbf{l} = \mathbf{m} \times \mathbf{n}$. Table 1 compares the unit vectors in GSM of the MVAB and unit vectors obtained from the Shue model. The vector **N** component from LMN and **n** component agree within an angle of ~18°; thus, we will use the LMN coordinate system for this study.

Table 1
MVAB and Shue Et Al. (1998) Model Results

(1) MVAB	(2) Shue et al.
N = *min* = [0.890, 0.153, −0.428]	**n** = [0.981, 0.152, −0.117]
M = *int* = [0.274, −0.931, 0.236]	**m** = [0.153, −0.988, 0.000]
L = *max* = [0.362, 0.328, 0.872]	**l** = [0.116, 0.018, 0.993]

The magnetopause crossing displays a sharp variation in the magnetic field strength and direction. Figure 1a shows the total magnetic field (Bt) and its components ($\mathbf{B}_{LMN}$). The total magnetic field Bt, represented by the black line, is strong and stable with values around 36 nT inside the magnetosphere, and the magnetic field vector points mostly in the northward $\mathbf{L}$ direction (before 07:04:25 UT—Line 3), while in the magnetosheath (after 07:06:10 UT—Line 7) the total field strength values decrease to approximately 15 nT. During the magnetopause crossing (between Lines 3 and 4), Bt reaches a minimum value of 0.7 nT. There is a rotation of the B_L component, represented by the blue line, from positive values inside the magnetosphere to negative values in the magnetosheath. Also, the B_M component, represented by the green line, changes its orientation across the magnetopause. After the magnetopause crossing, MMS3 observed a boundary layer (before Line 5) for approximately 30 s, where the values of B_L component are positive but lower than the values inside the magnetosphere (Line 1) followed by a full magnetosheath excursion (after Line 5). Plasma parameters also change drastically throughout the magnetopause crossing. Variations in the ion and electron bulk flows can be observed in Figures 1b and 1c (which will be discussed in detail later in this section). Figure 1d shows the expected increase of the number density for ions and electrons across the magnetopause from the magnetosphere and into the magnetosheath. Figure 1e shows the dominance of the magnetic pressure ($P_B = Bt^2/2\mu_0$) inside the magnetosphere, while the plasma thermal pressure ($P_{th} = nk_BT_{total}$, where k_B is the Boltzmann constant) dominates in the magnetosheath. Figures 1f and 1g show the energy spectra for ions and electrons, respectively. It is possible to distinguish the higher ($> \sim8$ keV) energy particle population inside the magnetosphere from the lower particle energy population in the magnetosheath region. During the magnetopause crossing and the boundary layer incursion, MMS observed a clear reconnection jet in the southward direction ($V_{iL} < 0$) with a negative V_{iM} (i.e., a duskward) component.

To identify magnetic reconnection, we compared the ion outflow jet (V_{jet}) with the hybrid Alfvén velocity (V_A) predicted by Cassak and Shay (2007). Asymmetric reconnection is identified when the jet speed is within 25% of the predicted hybrid Alfvén velocity (Walsh et al., 2014). The ion jet velocity is obtained by subtracting the reconnecting component of the exhaust velocity ($|V_{iL}| = 350$ km/s) at 07:05:10 UT from the background flow in the $\mathbf{L}$ direction at 07:07:30 UT ($|V_{background}| = 120$ km/s). The predicted ion Alfvén is determined by $V_A^2 = B_{Sh}B_{Sp}(B_{Sh}+B_{Sp})/\mu_0(\rho_{Sh}B_{Sp}+\rho_{Sp}B_{Sh})$, where $B = |B_L|$ is the reconnecting component of the magnetic field, ρ is the ion mass density, and the subscripts Sh and Sp correspond to the magnetosheath and magnetosphere, respectively. We choose times when the parameters are stable in the magnetosphere (07:03:30 UT) and in the magnetosheath (07:07:30 UT) to collect these values. For the respective values: [$B_{Sp} = 36$ nT, $n_{Sp} = 0.12$ cm^{-3}] and [$B_{Sh} = 16.5$ nT, $n_{Sh} = 8$ cm^{-3}], we found $V_A = 226$ km/s and $V_{jet} = 230$ km/s. The outflow jet and the predicted Alfén velocities are comparable, which is an evidence of the magnetic reconnection process.

After leaving the reconnection exhaust region, the MMS spacecraft observed an FTE with a clear and strong bipolar signature in the B_N component centered on an enhanced total magnetic field (Bt) in the magnetosheath at 07:06 UT (Lines 6 and 7 in Figure 1). The structure passed by the satellites very quickly, but it is well observed by the high-resolution MMS instruments. Other FTE-like structures (marked by small arrows) were also observed in the same region, at 07:07:51, 07:08:12, and 07:08:34 UT, just before the satellites crossed the magnetopause for the second time around 07:09:30 UT.

Figures 1h–1j show sequential magnetic field topologies that best describe the observations from 07:02:00 to 07:06:10 UT, when MMS cross the magnetopause from the magnetosphere ("Sp") to the magnetosheath ("Sh"). The black solid lines depict the magnetic field on both sides of the magnetopause. The arrows indicate the magnetic field orientation in the LN coordinate system plane. The cyan line indicates the MMS trajectory across the magnetopause. The MMS spacecraft are represented by the four colored dots, but for simplification the distances among them are out of scale. The numbers correspond to the features marked by the labeled dashed lines in Figures 1a–1g. MMS3 was initially in the magnetosphere, as described above, which is on the left side of Figure 1h. After Instant Number 2, MMS3 recorded a strong northward-dawnward electron jet ($+V_{eL}$, $+V_{eM}$) inside the magnetosphere on the order of 570 km/s denoted by the orange arrow. The strong northward electron jet near the magnetopause and the absence of ions moving in the same direction indicate the electron edge (Gosling et al., 1990; Øieroset et al., 2015) of a magnetic reconnection region located northward of the spacecraft. The electron edge is indicated by the orange solid line in Figure 1h. Nearer to the magnetopause at 07:04:20 UT, there is a reversal in the electron velocity (marked by Line 3) followed by a southward ion jet (red arrow) and the magnetopause crossing (between Instants 3 and 4). Just before Instant 4, B_L reverses to southward and Bt is minimum indicating that MMS3 crossed

the magnetopause current layer. In the sequence (between 4 and 5), B_L turns from positive to negative values at the same time that strong ion and electron southward jets are observed corresponding to the outflow region of a reconnection line located northward of the spacecraft location. The B_L rotation is interpreted as the forward and backward motion of the layer making MMS3 observe the magnetopause edge closer to the magnetosphere at the first moment (Line 4) and the subsequent observation of the edge closer to the magnetosheath (Line 5). Figure 1i corresponds to the instant when MMS3 is in the magnetosheath just before the FTE encounter. In this region, MMS3 did not observe reconnection jets but only the magnetosheath bulk flow. Figure 1j corresponds to the time after the FTE passes by MMS3, indicated by the blue arrow, with the negative-positive bipolar variation of B_N indicating southward motion of the structure. At this region the MMS spacecraft moves with speed of 1 km/s approximately, so the relative motion is due to the structures passing through the spacecraft. Note the time sequence of the events observed: reconnection jet—magnetosheath flow—FTE. There is no evidence of a reconnection line southward of MMS3 after the FTE is observed.

Also, assuming that an FTE formed by two reconnection lines is a closed structure, we expected to observe counterstreaming flows toward the center of the FTE from both reconnection lines. Similar signatures in the pitch angle are expected for multiple reconnection lines, where electrons streaming toward a line from the southern and northern sides as suggested by Hwang et al. (2018) and Øieroset et al. (2011). We will show later that ion and electron flows inside the FTE are only southward and the electron pitch angle distribution in Figures 2p and 2q show electrons streaming parallel to the magnetic field. We understand the pitch angle signature plus the absence of other reconnection signatures require us to invoke the single reconnection line model. Consequently, the FTE generation mechanism is consistent with an intensification of reconnection at a preexisting reconnection line and the formation of a southward moving bubble, as in the model of Southwood et al. (1988) and Scholer (1988).

3.2. FTE Structure and Motion

Figure 2 shows MMS3 observations from 07:06:00 to 07:06:08 UT. Similar signatures are clearly observed by all MMS spacecraft. Figure 2a shows a large negative-positive bipolar variation in the normal magnetic field component (B_N, red line), from –20 to 25 nT. The north-south component direction (B_L, blue line) depicts an enhancement to negative values ($\sim$ –38 nT). And the third component (B_M, green line) exhibits negative values close to the edges of the FTE and positive values at the center indicating a "W" shape at 07:06:04 UT. A W-shaped B_M signature is expected when crossing a flux rope with a strong core magnetic field in the dawn-dusk axial direction as suggested by Fear et al. (2012), which is consistent with a long reconnection line models. Figure 1b shows that the magnetosheath plasma bulk velocity is southward. The ion bulk flow velocity observed by MMS3 exhibited a southward enhancement ($\sim$ –280 km/s) during the FTE at 07:06:04 UT (-V_{iL}), which is consistent with the negative-positive B_N polarity indicating a southward moving FTE.

Accelerated flows are seen more clearly in the electron velocity, mainly in the V_{eL} component that indicates a strong southward enhancement at 07:06:03.8 UT in Figure 2c. Figure 2d shows the electric field. The E_N component exhibits positive values ($\sim$4 mV/m) outside the structure, that is, immediately to the left of the leftmost vertical dashed line. Right after, that is, from 07:06:02 UT onward, E_N changes to negative values ($\sim$ –5 mV/m) near the leading pulse (negative B_N variation) at 07:06:02 UT. In this region E_M increases to 6 mV/m and E_L fluctuates between $\pm$4 mV/m. Near the core of the FTE, that is, $\sim$07:06:04 UT E_N becomes positive reaching $\sim$10 mV/m, whereas E_M exhibit a positive to negative bipolar pulse inside the FTE from $\sim$7 to $\sim$ –10 mV/m. Electron and ion densities in Figure 2e show two depletions centered on the B_N peaks at 07:06:03.5 and 07:06:04.1 UT, but both increase again close to the center at 07:06:03.8 UT. However, the density of both species at the structure's core remains slightly lower than in the magnetosheath. Ion and electron temperatures are shown in Figures 2f and 2g). The ion temperature shows an enhancement inside the FTE for both the parallel and perpendicular components, whereas the electron temperature parallel to the magnetic field exhibits an increase in the core region and decrease in the edges. Akhavan-Tafti et al. (2019) show that particles are cooled at the trailing edge due to a relaxing field topology, which is consistent with the observation presented in this work.

The MMS tetrahedral formation enables current density determination using the curlometer technique (Dunlop et al., 2002; Robert et al., 1998). This technique is based on the assumption that this magnetic field varies linearly between the spacecraft in the tetrahedron to ensure a constant current over the spacecraft

Figure 2. (a–r) Magnetic field and plasma data showing the FTE observed by MMS3 during the time interval from 07:06:00 to 07:06:08 with data 1,024 data points. The vertical dashed lines indicate the negative and positive peaks of B_N.

volume. We employed the curlometer technique to determine the current density (CurlB) of the structure, which is shown by the red lines in Figures 2h–2j. The results can be compared with current densities from the FPI moments (black line in Figures 2h–2j), since $\mathbf{J}_{FPI} = n_q e(\mathbf{V}_e - \mathbf{V}_i)$ where n_q is the number density, assumed to be the same for ions and electrons, e is the elementary Coulomb charge, and $\mathbf{V}_e$ and $\mathbf{V}_i$ are the electron and ion velocities, respectively. Both results agree very well, demonstrating that variations in the current density are physical. The total current density (Figures 2h) exhibits a small peak (filament) just before the FTE's leading edge at 07:06:02.5 UT (just to the left of the leftmost vertical dashed line), a similar

peak was reported by Eastwood et al. (2016) but associated with the magnetopause edge of the structure. There is no similar structure on the trailing edge at 07:06:04.5 UT. The current has a large peak in the core of the FTE in the direction antiparallel to the magnetic field. Comparison between parallel and perpendicular components of the current shows that J_{para} is stronger than J_{perp} by a factor of 3, suggesting a nearly force-free nature for the structure. As expected, the FTE exhibits a pressure imbalance, with the magnetic pressure ($Bt^2/2\mu_0$) increasing in the structure's core while the thermal pressure ($n\kappa_B T_{total}$) decreases, resulting in an over pressure at the core as shown in Figure 2k. Following Equation 2 of Paschmann et al. (1982), we can estimate the pressure balance across the event: $\Delta(p + Bt^2/2\mu_0) = B_t(B_N^+ - B_N^-)/4\pi$, the first term is the total pressure variation inside and outside the FTE and the second term is an estimation of the magnetic curvature considering the Bt as the total field outside the FTE, and B_N^+ and B_N^- are the maximum and minimum values of B_N. Comparing both terms of the equation, it is found that the pressure gradient force is greater than the curvature force by a factor of 2, suggesting the structure is expanding. Figures 2l–2o show ion energy and pitch angle distributions. Particles with energies from 0.1 to 1 keV (n) and 1 to 30 keV (o) stream parallel to the magnetic field inside the FTE, in the region between the vertical dashed lines. The energy distribution and pitch angle for electrons exhibit a similar behavior as shown in Figures 2p–2r where electrons with energies from 200 eV to 2 keV flow aligned to the magnetic field. The streaming particle motion provides evidence that one end of the FTE is connected to the solar wind and the other to the southern ionosphere, consistent with the southward motion and generation below the reconnection line (Scholer, 1988).

Figures 3a–3d compare the magnetic field, electron flow speed (e–h), electric field (i–l), and the current density (m–p) obtained from the curlometer technique and FPI moments observed by all four MMS spacecraft during the FTE crossing. The magnetic features observed by the spacecraft are similar. The B_M components observed by MMS1 and MMS2 are slightly more intense than those seen by MMS3 and MMS4. No difference can be observed in the ion flow velocities (not shown here). However, a critical difference is observed in the V_{eM} component of the electron bulk flow (Figure 3g). Near the FTE center at 7:06:03.8 UT MMS1 and MMS2 observed positive values of V_{eM} around 570 and 255 km/s respectively, while MMS3 and MMS4 observed lower values of V_{eM} around -140 km/s. The influence of the electron bulk flow can be observed in both the electric field observation and in the current density calculated from the FPI moments. MMS1 and MMS2 observe a small values of E_N component close to the core of the FTE, whereas MMS3 and MMS4 observe peaks in E_N in the same region. This is also true for the J_M component observed by MMS1 and MMS2, as shown in panel o.

We subtracted the background magnetic field to analyze the FTE symmetry. We calculate the background magnetic field B_N = 4.6 nT before the FTE encounter between 07:05:51 and 07:05:57, when the magnetic field was more steady. We found that the leading pulse is stronger than the trailing pulse, –24.6 and 20.4 nT, respectively. The ratio between these values demonstrates that the FTE is an asymmetric structure. (Note: The magnetic field background has not been subtracted in Figure 3.) MMS3 and MMS4 spent more time crossing the FTE, that is, 1.61 and 1.63 s, respectively, from B_N peak to peak, than MMS1 and MMS2, which crossed both FTE's edges in 1.60 and 1.57 s, respectively. We can use the MMS spacecraft to estimate the FTE's speed (V_{FTE}) and direction of motion (Harvey, 1998). We considered the time and location differences between the Bt maximum observed by MMS1 and the other MMS spacecraft. The velocity can be obtained by $(\mathbf{r}_\alpha - \mathbf{r}_1) \cdot \hat{\mathbf{n}} = V_{FTE}(t_\alpha - t_1)$, where α indicates MMS 2, 3, and 4. Our analysis indicates that the FTE moved southward and duskward with a speed of V_{FTE} = 324 km/s and direction (–0.04, 0.15, –0.99) in GSM coordinates. When we consider the average time in which the spacecraft takes to go through the structure, the event has a cross section of 518 km.

The FTE's cross-section dimension can be compared with local characteristic plasma lengths such as the ion and electron inertial lengths di and de, respectively. Taking the ion and electron numerical densities in the magnetosheath region in the vicinity of the FTE as ∼7.7 cm^{-3}, the ion and electron inertial lengths are di = 82 km and de = 1.9 km, respectively. Therefore, the FTE's cross section would be about 6.3di, which is comparable to dimensions previous found for ion-scale flux ropes at the Earth's dayside magnetopause (e.g., Eastwood et al., 2016). In terms of the ion gyroradius ρ_i, the FTE's cross section would be ∼4.4ρ_i (ρ_i = 117.4 km). Also, we estimate the spatial dimension related to the region within the FTE's core where the electron bulk flow intensities departure significantly from background values. We then take the region, for both MMS1 and MMS2, where the electron total velocity (V_{et}) is higher than the surrounding values, and such a region is demarcated by the vertical dashed Lines 2 and 3. We define this region as the FTE core's cross section. Considering the time of about 0.56 s that MMS1 and MMS2 satellites took to cross the FTE
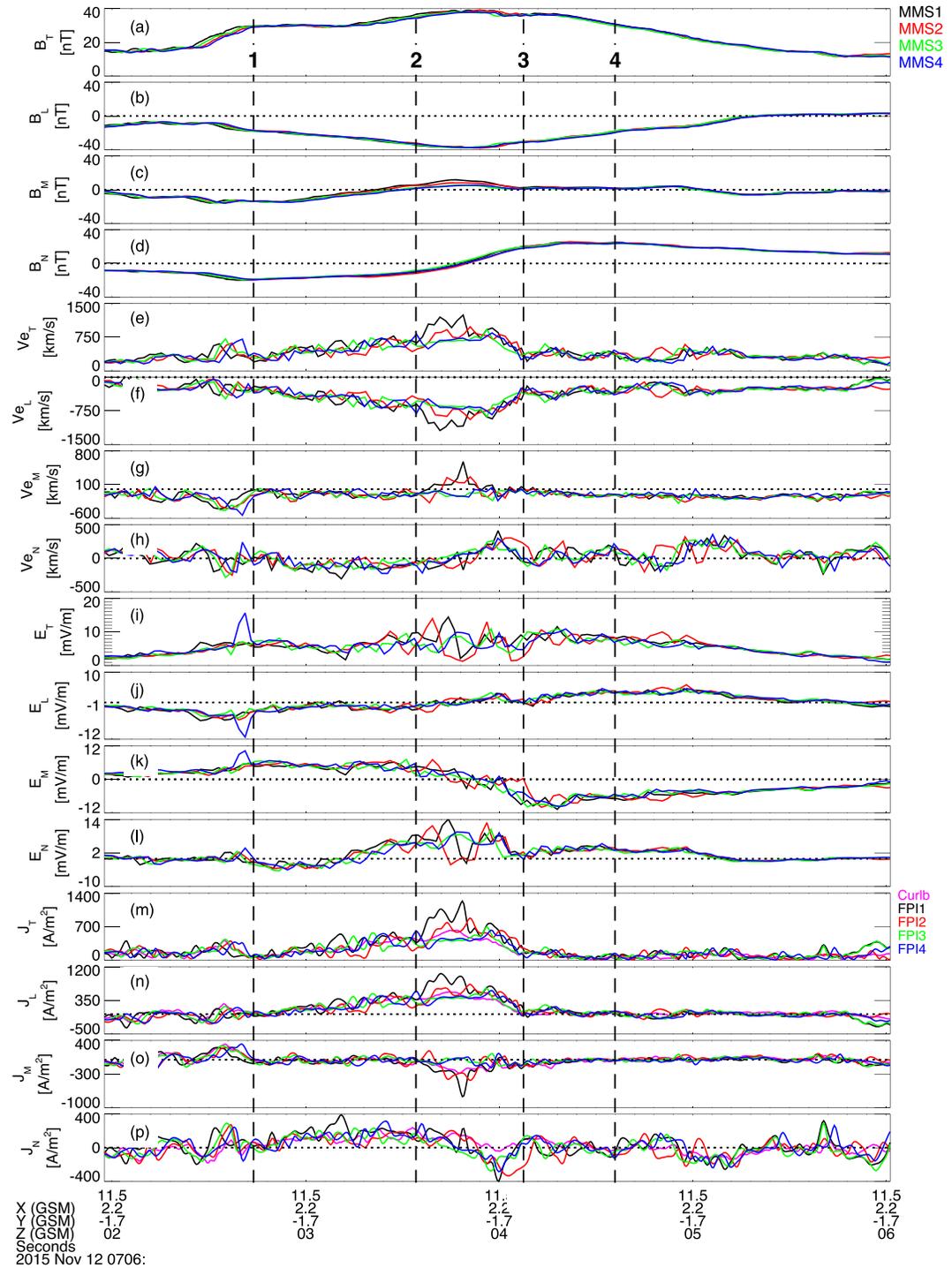
Figure 3. A comparison of magnetic field and plasma data in the time interval between 07:06:02 and 07:06:06 UT observed by all four MMS spacecraft, indicated by colors. The vertical dashed Lines 1 and 4 indicate the negative and positive peaks of B_N. Lines 2 and 3 show the time interval when MMS1 and MMS2 crossed the core of The FTE.
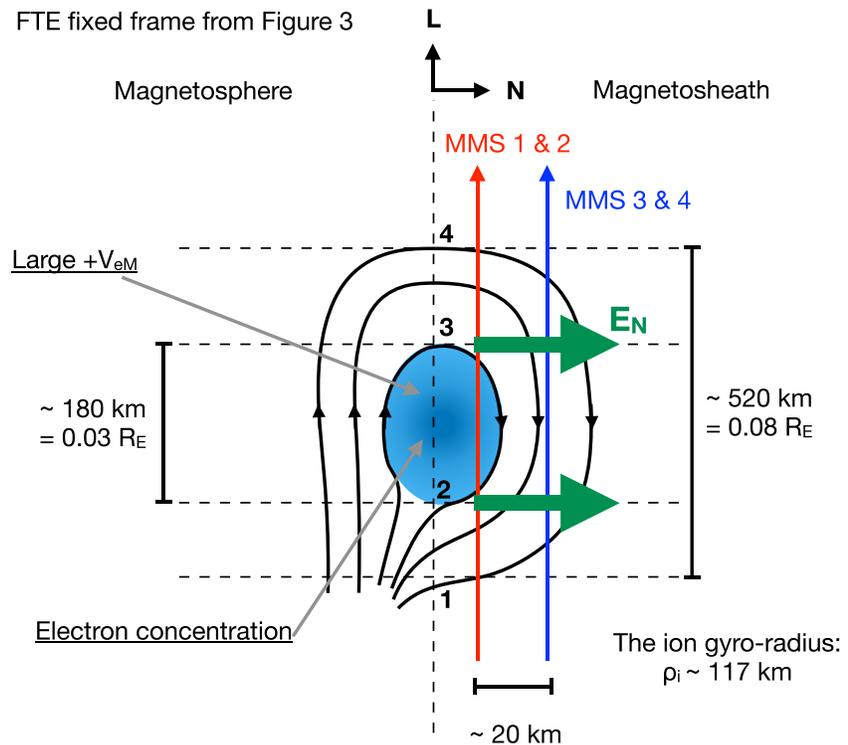
Figure 4. A sketch out of scale showing the MMS1 and MMS2 trajectories through the FTE's core where a strong V_{eM} is observed and MMS3 and MMS4 passing outside the core, observing the E_N component.

core's cross section, the inferred diameter is 181.4 km, which is only $2.2di$ and $\sim1.5\rho_i$. In terms of electron inertial length an electron gyroradius scales the FTE core's cross section is $95.5de$ and $221\rho_e$, respectively, where $de = 1.9$ km and $\rho_e = 0.82$ km.

4. Discussion and Conclusions

We presented MMS observations of an outbound magnetopause crossing. Magnetic reconnection was identified based on the accelerated ion and electron southward jets during the magnetopause crossing. Also, the strong southward magnetosheath magnetic field, making a shear angle of $\sim166°$ with the magnetospheric field is favorable for dayside magnetic reconnection near to subsolar region. A northward electron jet is observed on the magnetospheric side, indicating the satellites entered an electron layer south of the reconnection line. Nearer to the magnetopause, southward ion and electron jets indicate the satellites crossed the outflow region southern of the reconnection line. The ion jet was faster on the magnetosheath side. About 1.5 min after MMS crossed the magnetopause all spacecraft observed one very small FTE. The time sequence of the observation indicates that the FTE was generated by an intensification of reconnection at a preexisting reconnection line, which became bursty as suggested by Southwood et al. (1988) and Scholer (1988).

The FTE structure shows a large negative-positive bipolar variation in the magnetic field component (B_N) normal to the nominal magnetopause, from –20 to 25 nT, indicating a southward moving event. MMS observed enhanced southward ($-V_{iL}$) flow velocities consistent with the motion inferred from the negative-positive B_N polarity. The suprathermal electrons streaming aligned to the magnetic field are also consistent with the reconnection line location. Using the curlometer technique, we inferred a strong current antiparallel to the magnetic field inside the FTE. The field-aligned current is approximately 3 times higher than the perpendicular current inside the FTE, indicating that the FTE has an approximately force-free nature.

All four MMS spacecraft observed similar magnetic field signatures, including almost the same duration for the peak to peak FTE B_N signature (~1.6 s). A slight difference in the B_M components is observed, which may indicate that MMS1 and MMS2 crossed the FTE closer to its core than MMS3 and MMS4. These differences can also be observed in the electron flows, electric field measurements, and the current density calculated

from the FPI moments. MMS1 and MMS2 observe weak E_N components near the FTE's core, while MMS3 and MMS4 observe higher values for E_N during the same interval. The E_N suppression near the FTE's core observed by MMS1 and MMS2 can be explained as follows: Since $E = -V \times B$, the dawnward-southward electron flow plays a crucial role in generating E_N. Considering the E_N component, that is, $E_N = -(V_{eL}B_M - V_{eM}B_L)$. Inside the interval delimited by the dashed Lines 2 and 3 in Figure 3g for MMS1 and MMS2, the electron jet in V_{eM} changes direction and aligns with the core magnetic field direction. On the other hand, for MMS3 and MMS4 V_{eM} does not change; that is, it remains negative. It shows that E_N is balanced by the V_{eM} inside the core region. We claim that MMS1 and MMS2 crossed the FTE's core and MMS3 and MMS4 do not reach this region. Then, this can explain the differences observed in the electron V_{eM} component among the MMS spacecraft. In Figure 3l, E_N is suppressed near the FTE's core (black and red lines) showing that $V_{eM}B_L$ in the core region balances $V_{eL}B_M$. Figure 4 shows a schematic of the FTE structure for the present study. MMS1 and MM2 observed a strong V_{eM} jet only in the core region, which is between horizontal dashed Lines 2 and 3. These differences can also be inferred from the J_M component. MMS1 and MMS2 observe a stronger current than MMS3 and MMS4, which is reasonable since **J** is related to **V**e.

We used timing analysis to determine the FTE motion and speed. Our analysis indicates that the FTE moves southward with a speed of V_{FTE} = 324 km/s and direction (–0.04, 0.15, –0.99) southward and duskward. The FTE moves faster than the surrounding plasma bulk flow (∼150 km/s) and comparable with the ion plasma bulk flow inside the FTE (∼310 km/s). When we multiply V_{FTE} by the average time which the spacecraft takes to cross the structure, we find the cross section to be only 518 km. This FTE cross-section dimension also can be compared with characteristic local lengths. The ion and electrons number densities in the magnetosheath next to FTE are around 7.7 cm^{-3}, giving the ion and electron inertial lengths of 82 and 1.9 km, respectively. Therefore, the FTE cross section corresponds to 6.3 ion inertial lengths and 273 electron inertial lengths. Compared to the particle gyroradii of 117.4 km for ions and 0.82 km for electrons, the cross section is 4.4 and 631 ion and electron gyroradii, respectively. We consider the internal region to be the FTE's core, where electron velocities are affected and the current is more intense for MMS1 and MMS2. Using the structure velocity from timing analysis, we estimate a length of 181.4 km for the core region. In terms of ion and electron inertial length, the core dimension corresponds to 2.2 di and 95.5 de, respectively. When compared with ion and electron gyroradii, the core dimension corresponds to 1.5ρ_i and 221ρ_e, respectively. It is evident that the region is not large enough to affect the ion behavior, but it does for the electrons, showing that the FTE's core is an electron-scale structure. Our work reveals this new feature about FTEs, which could not be achieved during previous missions. MMS provides better resources to investigate layers of transient events and understanding of their formation and evolution.

Data Availability Statement

MMS data used in this study can be obtained online (from https://lasp.colorado.edu/mms/sdc/public/about/browse-wrapper/), and ACE data used in this study can be obtained from GSFC (https://cdaweb.gsfc.nasa.gov/index.html/).

References

Akhavan-Tafti, M., Slavin, J. A., Le, G., Eastwood, J. P., Strangeway, R. J., Russell, C. T., et al. (2018). MMS examination of FTEs at the Earth's subsolar magnetopause. *Journal of Geophysical Research: Space Physics*, *123*, 1224–1241. https://doi.org/10.1002/2017JA024681

Akhavan-Tafti, M., Slavin, J. A., Sun, W. J., Le, G., & Gershman, D. J. (2019). MMS observations of plasma heating associated with FTE growth. *Geophysical Research Letters*, *46*, 12,654–12,664. https://doi.org/10.1029/2019GL084843

Berchem, J., & Russell, C. T. (1984). Flux transfer events on the magnetopause: Spatial distribution and controlling factors. *Journal of Geophysical Research*, *89*(A8), 6689–6703. https://doi.org/10.1029/JA089iA08p06689

Birn, J., Artemyev, A. V., Baker, D. N., Echim, M., Hoshino, M., & Zelenyi, L. M. (2012). Particle acceleration in the magnetotail and aurora. *Space Science Reviews*, *173*(1–4), 49–102. https://doi.org/10.1007/s11214-012-9874-4

Burch, J. L., Moore, T. E., Torbert, R. B., & Giles, B. L. (2016). Magnetospheric Multiscale overview and science objectives. *Space Science Reviews*, *199*, 5–21. https://doi.org/10.1007/s11214-015-0164-9

Cassak, P. A., & Shay, M. A. (2007). Scaling of asymmetric magnetic reconnection: General theory and collisional simulations. *Physics of Plasmas*, *14*(10), 102114. https://doi.org/10.1063/1.2795630

Chen, L.-J., Bhattacharjee, A., Puhl-Quinn, P. A., Yang, H., Bessho, N., Imada, S., et al. (2008). Observation of energetic electrons within magnetic islands. *Nature Physics*, *4*, 19–23. https://doi.org/10.1038/nphys777

Drake, J. F., Swisdak, M., Che, H., & Shay, M. A. (2006). Electron acceleration from contracting magnetic islands during reconnection. *Nature*, *443*, 553–556. https://doi.org/10.1038/nature05116

Dungey, J. W. (1961). Interplanetary magnetic field and the auroral zones. *Physical Review Letters*, *6*(2), 47–48. https://doi.org/10.1103/PhysRevLett.6.47

Dunlop, M. W., Balogh, A., Glassmeier, K.-H., & Robert, P. (2002). Four-point cluster application of magnetic field analysis tools: The curlometer. *Journal of Geophysical Research*, *107*(A11), 1384. https://doi.org/10.1029/2001JA005088

Eastwood, J. P., Phan, T. D., Cassak, P. A., Gershman, D. J., Haggerty, C., Malakit, K., et al. (2016). Ion-scale secondary flux ropes generated by magnetopause reconnection as resolved by MMS. *Geophysical Research Letters*, *43*, 4716–4724. https://doi.org/10.1002/2016GL068747

Elphic, R. C. (2013). Observations of flux transfer events: Are FTEs flux ropes, islands, or surface waves? *Physics of magnetic flux ropes* (pp. 455–471). American Geophysical Union (AGU). https://doi.org/10.1029/GM058p0455

Ergun, R. E., Tucker, S., Westfall, J., Goodrich, K. A., Malaspina, D. M., Summers, D., et al. (2016). The axial double probe and fields signal processing for the MMS mission. *Space Science Reviews*, *199*(1), 167–188. https://doi.org/10.1007/s11214-014-0115-x

Escoubet, C. P., Fehringer, M., & Goldstein, M. (2001). Introduction: The Cluster mission. *Annales Geophysicae*, *19*(10/12), 1197–1200. https://doi.org/10.5194/angeo-19-1197-2001

Farrugia, C. J., Lavraud, B., Torbert, R. B., Argall, M., Kacem, I., Yu, W., et al. (2018). Magnetospheric Multiscale mission observations and non-force free modeling of a flux transfer event immersed in a super-Alfvénic flow. *Geophysical Research Letters*, *43*, 6070–6077. https://doi.org/10.1002/2016GL068758

Fear, R. C., Milan, S. E., Fazakerley, A. N., Lucek, E. A., Cowley, S. W. H., & Dandouras, I. (2008). The azimuthal extent of three flux transfer events. *Annales Geophysicae*, *26*(8), 2353–2369.

Fear, R. C., Milan, S. E., Fazakerley, A. N., Owen, C. J., Asikainen, T., Taylor, M. G., et al. (2007). Motion of flux transfer events: A test of the cooling model. *Annales Geophysicae*, *25*(7), 1669–1690. https://doi.org/10.5194/angeo-25-1669-2007

Fear, R. C., Milan, S. E., & Oksavik, K. (2012). Determining the axial direction of high-shear flux transfer events: Implications for models of FTE structure. *Journal of Geophysical Research*, *117*, A09220. https://doi.org/10.1029/2012JA017831

Fermo, R. L., Drake, J. F., Swisdak, M., & Hwang, K.-J. (2011). Comparison of a statistical model for magnetic islands in large current layers with Hall MHD simulations and Cluster FTE observations. *Journal of Geophysical Research*, *116*, A09226. https://doi.org/10.1029/2010JA016271

Fuselier, S. A., Lewis, W. S., Schiff, C., Ergun, R., Burch, J. L., Petrinec, S. M., & Trattner, K. J. (2016). Magnetospheric Multiscale science mission profile and operations. *Space Science Reviews*, *199*(1), 77–103. https://doi.org/10.1007/s11214-014-0087-x

Gonzalez, W. D., & Mozer, F. S. (1974). A quantitative model for the potential resulting from reconnection with an arbitrary interplanetary magnetic field. *Journal of Geophysical Research*, *79*, 4186–4194.

Gosling, J. T., Thomsen, M. F., Bame, S. J., Onsager, T. G., & Russell, C. T. (1990). The electron edge of low latitude boundary layer during accelerated flow events. *Geophysical Research Letters*, *17*(11), 1833–1836. https://doi.org/10.1029/GL017i011p01833

Harvey, C. C. (1998). Spatial gradients and the volumetric tensor. *ISSI Scientific Reports Series*, *1*, 307–322.

Heppner, J. P. (1972). Polar-cap electric field distributions related to the interplanetary magnetic field direction. *Journal of Geophysical Research*, *77*(25), 4877–4887. https://doi.org/10.1029/JA077i025p04877

Huang, S. Y., Jiang, K., Yuan, Z. G., Zhou, M., Sahraoui, F., Fu, H. S., et al. (2019). Observations of flux ropes with strong energy dissipation in the magnetotail. *Geophysical Research Letters*, *46*, 580–589. https://doi.org/10.1029/2018GL081099

Huang, S. Y., Sahraoui, F., Retino, A., Le Contel, O., Yuan, Z. G., Chasapis, A., et al. (2016). Mms observations of ion-scale magnetic island in the magnetosheath turbulent plasma. *Geophysical Research Letters*, *43*, 7850–7858. https://doi.org/10.1002/2016GL070033

Hwang, K.-J., Sibeck, D. G., Burch, J. L., Choi, E., Fear, R. C., Lavraud, B., et al. (2018). Small-scale flux transfer events formed in the reconnection exhaust region between two X lines. *Journal of Geophysical Research: Space Physics*, *123*, 8473–8488. https://doi.org/10.1029/2018JA025611

Hwang, K.-J., Sibeck, D. G., Giles, B. L., Pollock, C. J., Gershman, D., Avanov, L., et al. (2016). The substructure of a flux transfer event observed by the MMS spacecraft. *Geophysical Research Letters*, *43*, 9434–9443. https://doi.org/10.1002/2016GL070934

Jasinski, J. M., Slavin, J. A., Arridge, C. S., Poh, G., Jia, X., Sergis, N., et al. (2016). Flux transfer event observation at Saturn's dayside magnetopause by the Cassini spacecraft. *Geophysical Research Letters*, *43*, 6713–6723. https://doi.org/10.1002/2016GL069260

Jiang, K., Huang, S. Y., Yuan, Z. G., Yu, X. D., Liu, S., Deng, D., & He, L. H. (2019). Observations of whistler waves in two sequential flux ropes at the magnetopause. *Astrophysics and Space Science*, *364*(10), 168. https://doi.org/10.1007/s10509-019-3647-4

Lee, L. C., & Fu, Z. F. (1985). A theory of magnetic flux transfer at the Earth's magnetopause. *Geophysical Research Letters*, *12*(2), 105–108. https://doi.org/10.1029/GL012i002p00105

Lindqvist, P.-A., Olsson, G., Torbert, R. B., King, B., Granoff, M., Rau, D., et al. (2016). The spin-plane double probe electric field instrument for MMS. *Space Science Reviews*, *199*(1), 137–165. https://doi.org/10.1007/s11214-014-0116-9

Lockwood, M., & Smith, M. F. (1994). Low and middle altitude cusp particle signatures for general magnetopause reconnection rate variations: 1. theory. *Journal of Geophysical Research: Space Physics*, *99*(A5), 8531–8553. https://doi.org/10.1029/93JA03399

Mauk, B. H., Blake, J. B., Baker, D. N., Clemmons, J. H., Reeves, G. D., Spence, H. E., et al. (2016). The energetic particle detector (EPD) investigation and the energetic ion spectrometer (EIS) for the Magnetospheric Multiscale (MMS) mission. *Space Science Reviews*, *199*(1), 471–514. https://doi.org/10.1007/s11214-014-0055-5

Øieroset, M., Phan, T. D., Eastwood, J. P., Fujimoto, M., Daughton, W., Shay, M. A., et al. (2011). Direct evidence for a three-dimensional magnetic flux rope flanked by two active magnetic reconnection X lines at Earth's magnetopause. *Physical Review Letters*, *107*, 165,007. https://doi.org/10.1103/PhysRevLett.107.165007

Øieroset, M., Phan, T. D., Gosling, J. T., Fujimoto, M., & Angelopoulos, V. (2015). Electron and ion edges and the associated magnetic topology of the reconnecting magnetopause. *Journal of Geophysical Research: Space Physics*, *120*, 9294–9306. https://doi.org/10.1002/2015JA021580

Owen, C. J., Fazakerley, A. N., Carter, P. J., Coates, A. J., Krauklis, I. C., Szita, S., et al. (2001). Cluster peace observations of electrons during magnetospheric flux transfer events. *Annales Geophysicae*, *19*(10/12), 1509–1522. https://doi.org/10.5194/angeo-19-1509-2001

Paschmann, G., Haerendel, G., Papamastorakis, I., Sckopke, N., Bame, S. J., Gosling, J. T., & Russell, C. T. (1982). Plasma and magnetic field characteristics of magnetic flux transfer events. *Journal of Geophysical Research*, *87*(A4), 2159–2168. https://doi.org/10.1029/JA087iA04p02159

Paschmann, G., Øieroset, M., & Phan, T. (2013). In-situ observations of reconnection in space. *Space Science Reviews*, *178*(2–4), 385–417. https://doi.org/10.1007/s11214-012-9957-2

Phan, T. D., Dunlop, M. W., Paschmann, G., Klecker, B., Bosqued, J. M., Rème, H., et al. (2004). Cluster observations of continuous reconnection at the magnetopause under steady interplanetary magnetic field conditions. *Annales Geophysicae*, *22*(7), 2355–2367. https://doi.org/10.5194/angeo-22-2355-2004

Pollock, C., Moore, T., Jacques, A., Burch, J., Gliese, U., Saito, Y., et al. (2016). Fast plasma investigation for Magnetospheric Multiscale. *Space Science Reviews*, *199*(1), 331–406. https://doi.org/10.1007/s11214-016-0245-4

Priest, E., & Forbes, T. (2000). *Magnetic reconnection*. E. F. Priest (Ed.). Cambridge: Cambridge University Press.

Retinò, A., Bavassano Cattaneo, M. B., Marcucci, M. F., Vaivads, A., André, M., Khotyaintsev, Y., et al. (2005). Cluster multispacecraft observations at the high-latitude duskside magnetopause: Implications for continuous and component magnetic reconnection. *Annales Geophysicae*, *23*(2), 461–473. https://doi.org/10.5194/angeo-23-461-2005

Rijnbeek, R. P., Cowley, S. W. H., Southwood, D. J., & Russell, C. T. (1982). Observations of reverse polarity flux transfer events at the Earth's dayside magnetopause. *Nature*, *300*, 23–26. https://doi.org/10.1038/300023a0

Rijnbeek, R. P., Cowley, S. W. H., Southwood, D. J., & Russell, C. T. (1984). A survey of dayside flux transfer events observed by ISEE 1 and 2 magnetometers. *Journal of Geophysical Research*, *89*(A2), 786–800. https://doi.org/10.1029/JA089iA02p00786

Robert, P., Dunlop, M. W., Roux, A., & Chanteur, G. (1998). Accuracy of current density determination. *ISSI Scientific Reports Series*, *1*, 395–418.

Russell, C. (1995). A study of flux transfer events at different planets. *Advances in Space Research*, *16*(4), 159–163. https://doi.org/10.1016/0273-1177(95)00224-3

Russell, C. T., Anderson, B. J., Baumjohann, W., Bromund, K. R., Dearborn, D., Fischer, D., et al. (2016). The Magnetospheric Multiscale magnetometers. *Space Science Reviews*, *199*, 189–256. https://doi.org/10.1007/s11214-014-0057-3

Russell, C. T., & Elphic, R. C. (1978). Initial ISEE magnetometer results: Magnetopause observations (Article published in the special issues: Advances in magnetospheric physics with GEOS-1 and ISEE-1 and 2.) *Space Science Reviews*, *22*(6), 681–715. https://doi.org/10.1007/BF00212619

Russell, C. T., & Elphic, R. C. (1979). ISEE observations of flux transfer events at the dayside magnetopause. *Geophysical Research Letters*, *6*, 33–36. https://doi.org/10.1029/GL006i001p00033

Sanny, J., Tapia, J. A., Sibeck, D. G., & Moldwin, M. B. (2002). Quiet time variability of the geosynchronous magnetic field and its response to the solar wind. *Journal of Geophysical Research*, *107*(A12), 1443. https://doi.org/10.1029/2002JA009448

Saunders, M. A., Russell, C. T., & Sckopke, N. (1984). A Dual-satellite study of the spatial properties of FTEs. In E. W. Hones Jr. (Ed.), *Magnetic reconnection in space and laboratory plasmas* (pp. 145–152). Washington, DC: AGU.

Scholer, M. (1988). Magnetic flux transfer at the magnetopause based on single X line bursty reconnection. *Geophysical Research Letters*, *15*(4), 291–294. https://doi.org/10.1029/GL015i004p00291

Shue, J.-H., Song, P., Russell, C. T., Steinberg, J. T., Chao, J. K., Zastenker, G., et al. (1998). Magnetopause location under extreme solar wind conditions. *Journal of Geophysical Research*, *103*(A8), 17,691–17,700. https://doi.org/10.1029/98JA01103

Sibeck, D. G., & Lin, R.-Q. (2010). Concerning the motion of flux transfer events generated by component reconnection across the dayside magnetopause. *Journal of Geophysical Research*, *115*, A04209. https://doi.org/10.1029/2009JA014677

Smith, M. F., Rodgers, D. J., Rijnbeek, R. P., Southwood, D. J., Coates, A. J., & Johnstone, A. D. (1986). Plasma and field observations with high time resolution in flux transfer events. In Y. Kamide, & J. A. Slavin (Eds.), *Solar wind magnetosphere coupling* (Vol. 126, pp. 321–329).

Sonnerup, B. U. O., & Scheible, M. (1998). Minimum and maximum variance analysis. In G. Paschmann, & P. W. Daly (Eds.), *Analysis methods for multi-spacecraft data* (Vol. 1, pp. 185–220). Bern, Switzerland: The International Space Science Institute.

Southwood, D. J., Farrugia, C. J., & Saunders, M. A. (1988). What are flux transfer events? *Planetary and Space Science*, *36*, 503–508. https://doi.org/10.1016/0032-0633(88)90109-2

Stone, E. C., Frandsen, A. M., Mewaldt, R. A., Christian, E. R., Margolies, D., Ormes, J. F., & Snow, F. (1998). The Advanced Composition Explorer. *Space Science Reviews*, *86*, 1–22. https://doi.org/10.1023/A:1005082526237

Tsyganenko, N. A. (1996). Effects of the solar wind conditions in the global magnetospheric configurations as deduced from data-based field models (Invited). In *International conference on substorms* E. J. Rolfe, & B. Kaldeich (Eds.). (Vol. 389, p. 181).

Walsh, B. M., Phan, T. D., Sibeck, D. G., & Souza, V. M. (2014). The plasmaspheric plume and magnetopause reconnection. *Geophysical Research Letters*, *41*, 223–228. https://doi.org/10.1002/2013GL058802

Zhao, C., Russell, C. T., Strangeway, R. J., Petrinec, S. M., Paterson, W. R., Zhou, M., et al. (2016). Force balance at the magnetopause determined with MMS: Application to flux transfer events. *Geophysical Research Letters*, *43*, 11,941–11,947. https://doi.org/10.1002/2016GL071568

Zhong, Z. H., Tang, R. X., Zhou, M., Deng, X. H., Pang, Y., Paterson, W. R., et al. (2018). Evidence for secondary flux rope generated by the electron Kelvin-Helmholtz instability in a magnetic reconnection diffusion region. *Physical Review Letters*, *120*, 75101. https://doi.org/10.1103/PhysRevLett.120.075101